ASTRONOMY & ASTROPHYSICS
SUPPLEMENT SERIES

Astron. Astrophys. Suppl. Ser. **111,** 95-114 (1995)

Studies of dense molecular cores in regions of massive star formation.
II. CS $J = 2 - 1$ survey of southern H_2O masers in the longitude range $l = 260° - 310°$⋆,⋆⋆

I. Zinchenko[1,2], K. Mattila[2] and M. Toriseva[2]

[1] Institute of Applied Physics of the Russian Academy of Sciences, 46 Uljanov str., 603600 Nizhny Novgorod, Russia
[2] Helsinki University Observatory, Tähtitorninmäki, P.O.Box 14, FIN-00014 University of Helsinki, Finland

Received July 29; accepted December 8, 1994

Abstract. — We searched for the CS $J = 2 - 1$ emission towards 30 southern H_2O and OH masers with the SEST radio telescope (29 H_2O and H_2O/OH masers and 1 OH maser). We detected and mapped 24 CS emitting regions associated probably with 27 H_2O masers. The $C^{34}S$ $J = 2 - 1$ and CO $J = 1 - 0$ lines were also observed at the grid positions closest to the CS peaks. Here we present the CS maps and the spectra at the peak positions along with the CO and $C^{34}S$ spectra. We derive the $C^{34}S$ column densities in the LTE approximation and discuss briefly the spatial and kinematic structure of the sources. The association with the IRAS point sources and small scale structure sources is examined. We estimate the kinematic distances to the cores and derive their sizes, masses and mean densities. The velocity differences between the masers and CS cores are analyzed. The CO and CS spectra towards several sources demonstrate deep absorption features. We argue that they can be due to extended low excitation foreground cloud(s).

Key words: masers — stars: formation — ISM: clouds — ISM: molecules — radio lines: interstellar

1. Introduction

There is an increasing interest to systematic studies of dense molecular cores in regions of high mass star formation (HMSF). In comparison with low mass star forming regions, extended samples of which have been observed in various molecular lines, only a few, rather arbitrarily selected cores associated with HMSF regions have been investigated in some detail (for a review see e.g. Walmsley & Güsten 1994).

The goal of this project is to perform a systematic search for HMSF cores in the southern sky ($\delta < -30°$) and to start a thorough investigation of their properties. It continues the line started in our previous paper on the CS studies of 11 northern cores (Zinchenko et al. 1994, hereafter Paper I).

In the present study we selected H_2O masers as indicators of the regions of HMSF. They are known to be good pointers of such regions (e.g. Plume et al. 1992) due to their frequent association with them and their relatively accurate positions. The source list was compiled from the catalogue of non-stellar molecular maser sources published by Braz & Epchtein (1983), with additions from Braz et al. (1989) and Scalise et al. (1989). A similar study in the northern sky has been started by Plume et al. (1992, 1993).

In this paper we present the results of our $J = 2-1$ CS and $C^{34}S$ as well as $J = 1-0$ CO observations towards 30 H_2O and OH masers in the longitude range $260° - 310°$. We have mapped all detected cores in the CS line. The $C^{34}S$ and CO observations are limited to the positions of the CS emission peaks.

The structure of the paper is as follows: In Sect. 2 we describe the observations and data analysis. In Sect. 3 we present the observational results. In Sect. 4 we derive some physical parameters of the sources and discuss their properties. In Sect. 5 we present our conclusions.

Send offprint requests to: K. Mattila
⋆Based on the observations collected at the European Southern Observatory, La Silla, Chile
⋆⋆Tables 1 to 4 are also available in electronic form at the CDS via anonymous ftp 130.79.128.5

2. Observations and data analysis

2.1. *Observational procedure*

The observations were performed in October 1993 with the 15-m SEST telescope on La Silla, Chile. The telescope and its instrumentation are described by Booth et al. (1989). The half-power beamwidth of the telescope is 50″ at the CS and $C^{34}S$ frequencies (97981.00 MHz and 96412.98 MHz, respectively) and 45″ at the CO frequency (115.3 GHz). The front-end was a 3 mm Schottky mixer receiver. The single side band system temperature referred to outside the atmosphere was 400–500 K for CS, 320–340 K for $C^{34}S$ and 800–1000 K for the CO observations. The backend was a 2000 channel acousto-optical spectrometer with a 100 MHz bandwidth, 43 kHz channel separation and 80 kHz resolution. We smoothed the spectra to 86 kHz resolution which corresponds to 0.26 km/s for CS and $C^{34}S$ and 0.22 km/s for CO.

The observations were made mainly in the frequency switching mode with the frequency offset of 12 MHz. The CS spectra at the peak positions and a part of the $C^{34}S$ spectra were obtained with position switching. Initially, 3×3 point CS maps with 40″ spacing were obtained for all sources. Then, the mapping was continued according to the initial results and extended normally to ~ 10 % of the peak antenna temperature value. Pointing was checked periodically by observations of nearby SiO masers; the pointing accuracy was $\sim 5''$.

The standard chopper-wheel technique was used for the calibration. We express the results in the units of main beam brightness temperature ($T_{\rm mb}$) assuming the main beam efficiency ($\eta_{\rm mb}$) of 0.73 and 0.70 at the CS and CO frequencies, respectively (The SEST Handbook 1993). The temperature scale was checked by observations of Orion A and M17 SW.

2.2. *Source list*

The source list (Table 1) was compiled from the catalogue of non-stellar molecular maser sources published by Braz & Epchtein (1983), with additions from Braz et al. (1989) and Scalise et al. (1989). It includes masers with $\delta < -30°$. The present observations were limited to the longitude range $l = 260° - 310°$ (approximately). The maser coordinates are given in Table 1 where their uncertainties, if available, are also indicated (Col. 4). Twenty nine of these objects are H_2O or H_2O/OH masers and one is an OH maser only. In Cols. (5, 6) we present the galacto-centric distances and heights above the galactic plane based on the kinematic distances (Col. 7) as calculated from our $C^{34}S$ velocities (for the description of these calculations see Sect. 2.3). We give both near and far kinematic distances when appropriate. For some sources no solution could be found in the framework of the kinematic model which we used. In most cases spectrophotometric distances of the exciting stars of nearby H II regions have been published. They are indicated in Col. (8). It is worth noting that the association of these H II regions with the CS cores should be investigated in detail because the positional and velocity differences for some of them are rather large. In Col. (9) we present the radial velocities of the masers as given by the above mentioned authors.

2.3. *Data reduction and analysis*

We have reduced the data and produced maps using the GAG (*Groupe d'Astrophysique de Grenoble*) software package. The measured spectra were fitted by one or more gaussian components.

The next step in the data analysis was the derivation of the beam-averaged $C^{34}S$ column densities. We have performed it in the LTE approximation. The electric dipole moment was taken to be $\mu = 1.96$ D (Winnewisser & Cook 1968). The column densities were found from the $C^{34}S$ line intensity integral assuming for the excitation temperature the value $T_{\rm ex} = 10$ K (the dependence of the N_L(CS) estimates on the assumed $T_{\rm ex}$ is rather weak).

We have calculated kinematic distances to our sources from the $C^{34}S$ velocities according to the recommendations by Fich et al. (1989), i.e. for a flat rotation curve with $\Theta_0 = 220$ km/s assuming a standard IAU value for R_0 of 8.5 kpc.

3. Observational results

We detected the CS emission in most of our survey directions. In some cases we found that two masers are located within or very close to a single CS emission region. In total 24 such separate CS sources have been detected associated probably with 27 masers.

No noticeable CS emission has been detected towards G 284.17–0.79 (OH maser only), G 284.30–0.34 and G 299.02+0.15. A typical rms noise in the spectra was ~ 0.15 K.

In Fig. 1 we present the contour maps of the CS emission. The mapping grid positions as well as the positions of the H_2O masers and point IRAS sources are indicated. We constructed 4 maps for each source: a map of CS emission intensity integrated over the total velocity range and maps for 3 velocity intervals obtained by dividing the total interval into 3 equal parts. Thus, these maps give an impression of the source kinematics. To determine the total velocity range a composite spectrum was constructed for each source by overlaying all the measured spectra in one plot. Then, by visual inspection of this composite spectrum the velocity range was determined as the interval where a noticeable emission was present above the 3σ level (corresponding to ~ 0.4 K). In fact, significantly more extended wings can be seen in the spectra measured at the grid positions closest to the peaks of the CS emission which were obtained with a higher signal-to-noise ratio (Fig. 2). However, our data do not enable us

Table 1. Source list

Name	α(1950) (^{h}) (^{m}) (^{s})	δ(1950) (°) (′) (″)	$\Delta\theta$ (″)	R (kpc)	z (pc)	d (kpc)	d_{star} (kpc)	V_{H_2O} (km/s)	Remarks
G 261.64−2.09	08 30 23.2	−43 03 31		9.2	−86	2.4		8	
G 264.28+1.48	08 54 39.0	−42 53 30	30	8.8	36	1.4	2.9[a]	11	
G 265.14+1.45	08 57 36.3	−43 33 38	40	8.8	43	1.7		9	
G 267.94−1.06	08 57 21.7	−47 19 04	12	8.6	−12	0.7	1.7[b]	−3	
G 268.42−0.85	09 00 12.1	−47 32 07		8.6	−19	1.3	0.8[a]	−59	
G 269.11−1.12	09 01 45.	−48 14 00	30	8.9	−51	2.6	1.8[b]	5	
G 269.16−1.14	09 01 51.6	−48 16 43		8.9	−51	2.6	1.8[b]	18	
G 270.26+0.83	09 14 58.	−47 44 00	30	8.9	38	2.6	3.4[a], 2.2[b]	9	
G 284.17−0.79	10 19 42.	−57 50 06	60					(−25, +14)	OH only
G 284.30−0.34	10 22 20.	−57 32 00					2.3[a], 2.9[b]	7	
G 284.36−0.42	10 22 20.9	−57 37 48	12	8.7	−36	4.9	2.3[a], 2.9[b]	7	
G 285.26−0.05	10 29 36.8	−57 46 40	12	8.6	−4	4.7		3	
G 286.20+0.17	10 36 34.8	−58 03 22						−20	
G 287.38−0.62	10 41 39.	−59 19 00					2.8[b], 2.6[c]	−20	
G 289.95−0.89	10 59 07.4	−60 40 54		10.0	−139	8.9	6.0[b], 7.9[c]	24	
G 291.27−0.71	11 09 42.	−61 01 55	20				2.7[a], 2.8[b], 2.5[c]	−32	
G 291.28−0.71	11 09 47.2	−61 02 30	15				2.7[a], 2.8[b], 2.5[c]	−123	
G 290.37+1.66	11 10 07.4	−58 30 00					2.9[a]	−21	
G 291.57−0.43	11 12 54.	−60 52 57	12	9.0	−56	7.5	7.7[b], 7.2[c]	14	
G 291.64−0.56	11 13 03.5	−61 01 55	30	9.1	−74	7.6	7.7[b], 7.2[c]	−4	
G 294.51−1.62	11 33 12.9	−62 58 15		7.8	−66/−133	2.3/4.7	2.1[b]	−12	
G 294.97−1.73	11 36 51.6	−63 12 09		8.1	−35/−182	1.2/6.0	2.4[c]	−4	
G 298.22−0.34	12 07 22.	−62 33 20	40	10.2	−65	11.0		24	
G 299.02+0.15	12 14 44.5	−62 11 14						25	
G 300.97+1.14	12 32 00.2	−61 23 44	12				2.0[b]	−63	
G 301.12−0.20	12 32 31.3	−62 44 38						−42	
G 305.20+0.21	13 07 59.9	−62 18 50	12				3.9[b], 2.5[c]	−41	
G 305.36+0.15	13 09 21.0	−62 21 43	12	7.0	16/21	4.2/5.6	3.9[b], 2.5[c]	−37	
G 305.36+0.21	13 09 21.2	−62 18 02	12	7.0	16/21	4.2/5.6	3.9[b], 2.5[c]	−37	
G 308.80−0.25	13 13 27.2	−62 42 56		7.1	−13/−34	2.9/7.8		−39	

[a]Brand & Blitz (1993)
[b]Avedisova & Palouš (1989)
[c]Georgelin & Georgelin (1976)

to investigate the spatial structure of this wing emission. In Fig. 2 also the $C^{34}S$ and CO spectra at the same positions are displayed (in G 265.14+1.45 and G 291.64−0.56 the CO spectra were obtained at the maser positions). The atmospheric CO line is not noticeable in our spectra.

The CS and $C^{34}S$ spectra presented in Fig. 2 were fitted by gaussian curves. We found that in most cases single gaussians do not provide an acceptable fit for the CS spectra. Usually much better fit could be obtained with two-component fitting. The results of this procedure for the CS and $C^{34}S$ spectra are presented in Table 2. We consider these gaussian fits only as convenient numerical representations of the line profiles indicating their complex velocity structure, self-absorption, etc. We do not attempt to give a physical interpretation here. For derivation of the column densities and related parameters the line areas are more useful and we present them in Cols. (4) and (8) of Table 2. In Col. (12) the peak CO main beam brightness temperatures are given.

4. Discussion

4.1. *Detection statistics and associations with the IRAS sources*

As mentioned earlier we detected the CS emission in the vicinity of 27 (out of 29) H_2O masers in our sample and this emission comprises 24 separate regions altogether. Also the $C^{34}S$ line was detected in all these sources. Nothing was detected towards G 284.17−0.79 which contains only an OH maser, and towards 2 H_2O masers. The histograms of line area distributions for CS and $C^{34}S$ for the source peak positions are presented in Fig. 3. These distributions should not be much affected by the system sensitivity because the lines were detected in almost all

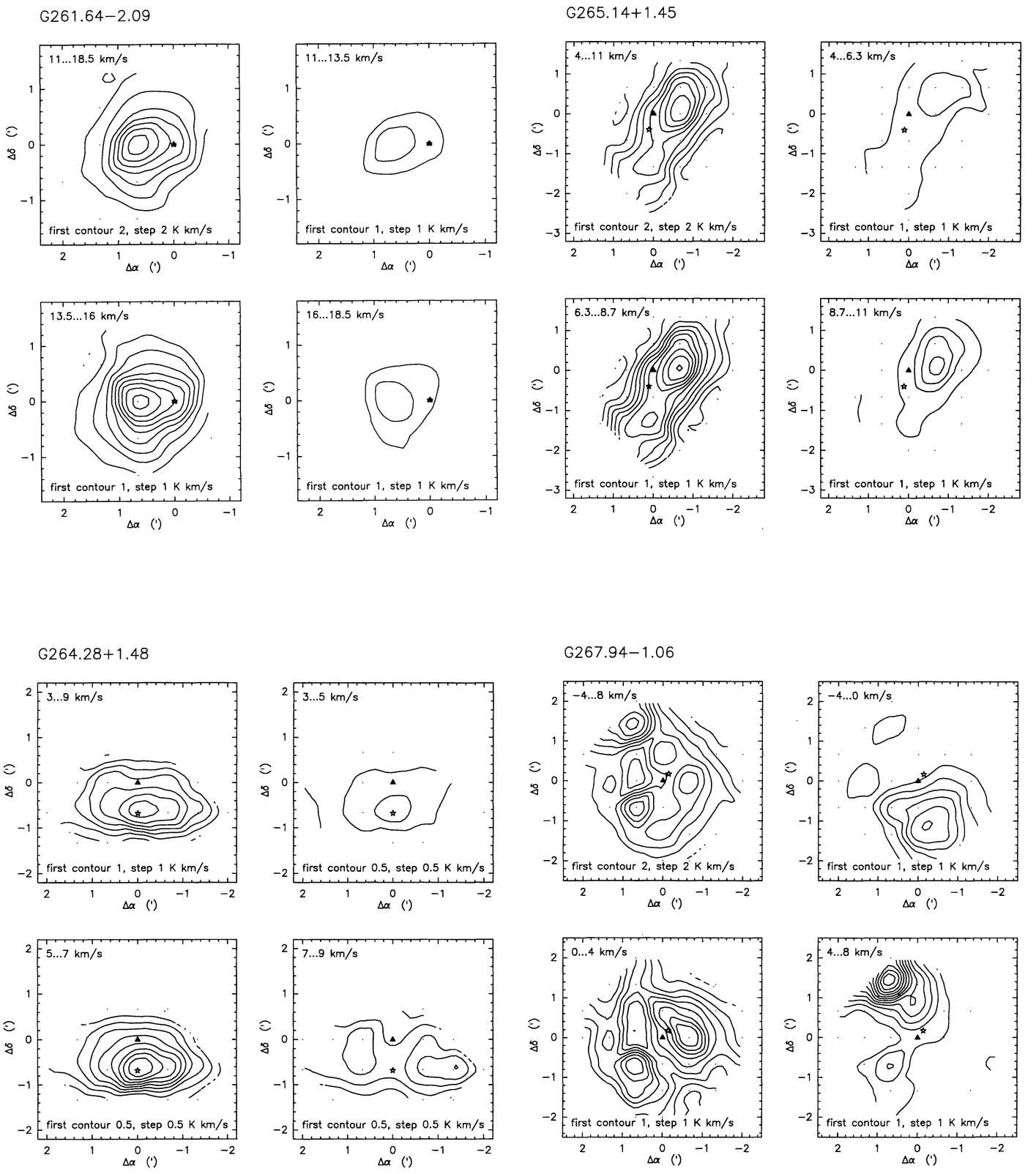

Fig. 1. The line area contour maps of the sources in the CS $J = 2 - 1$ line in the indicated velocity intervals. The dots indicate the observed positions. The asterisks show the positions of the IRAS point sources. The triangles mark the positions of the H_2O masers

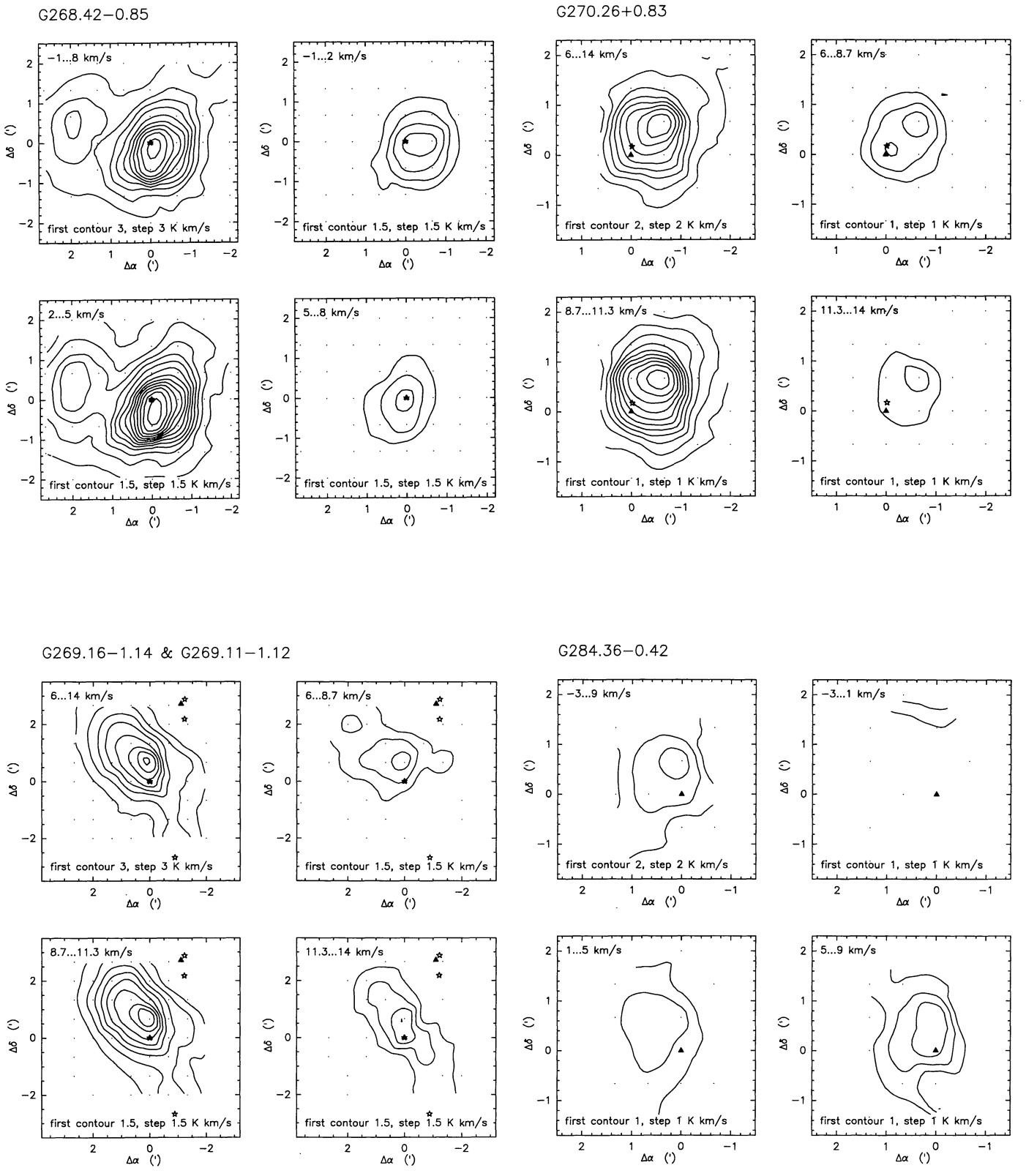

Fig. 1. continued

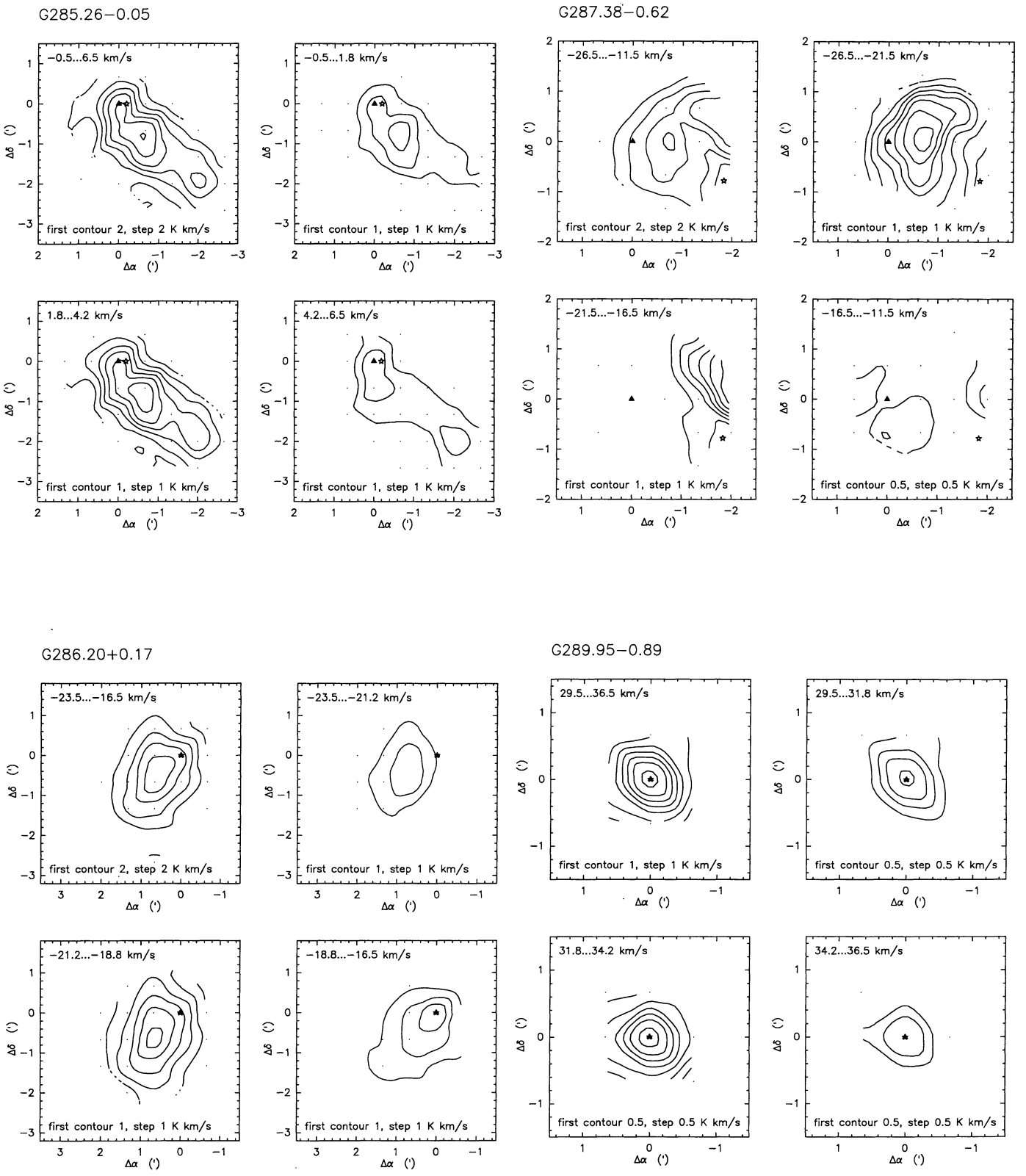

Fig. 1. continued

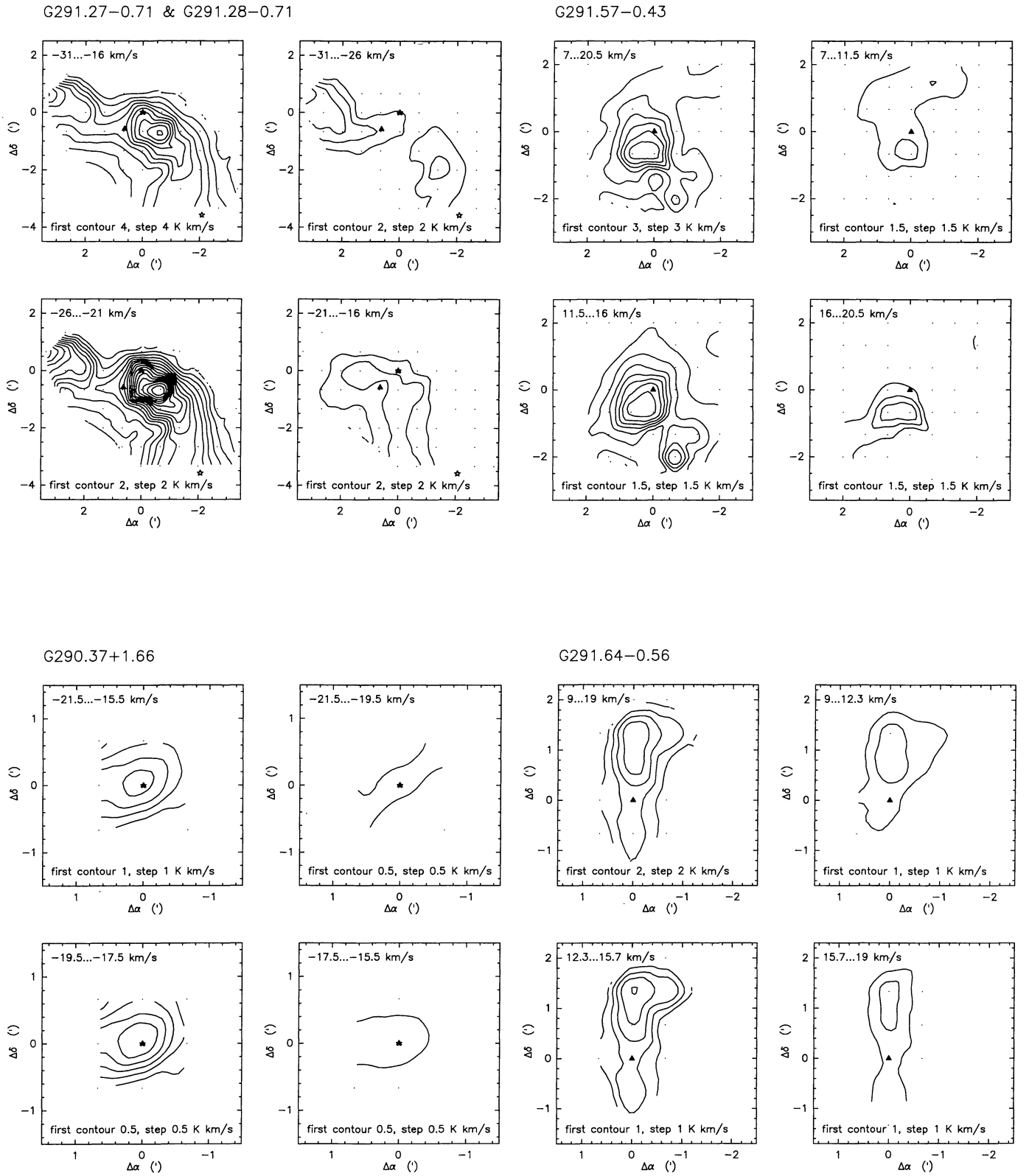

Fig. 1. continued

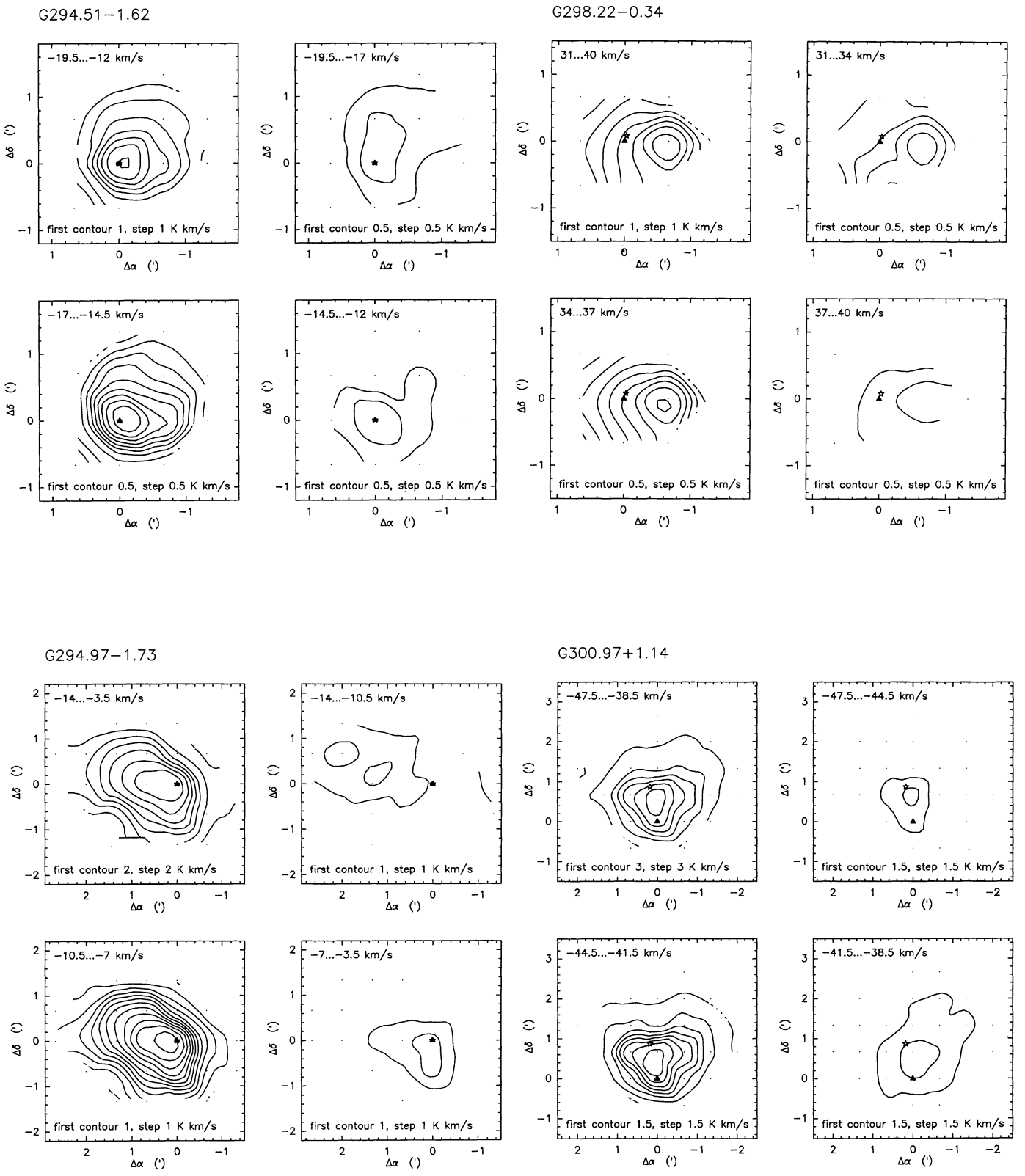

Fig. 1. continued

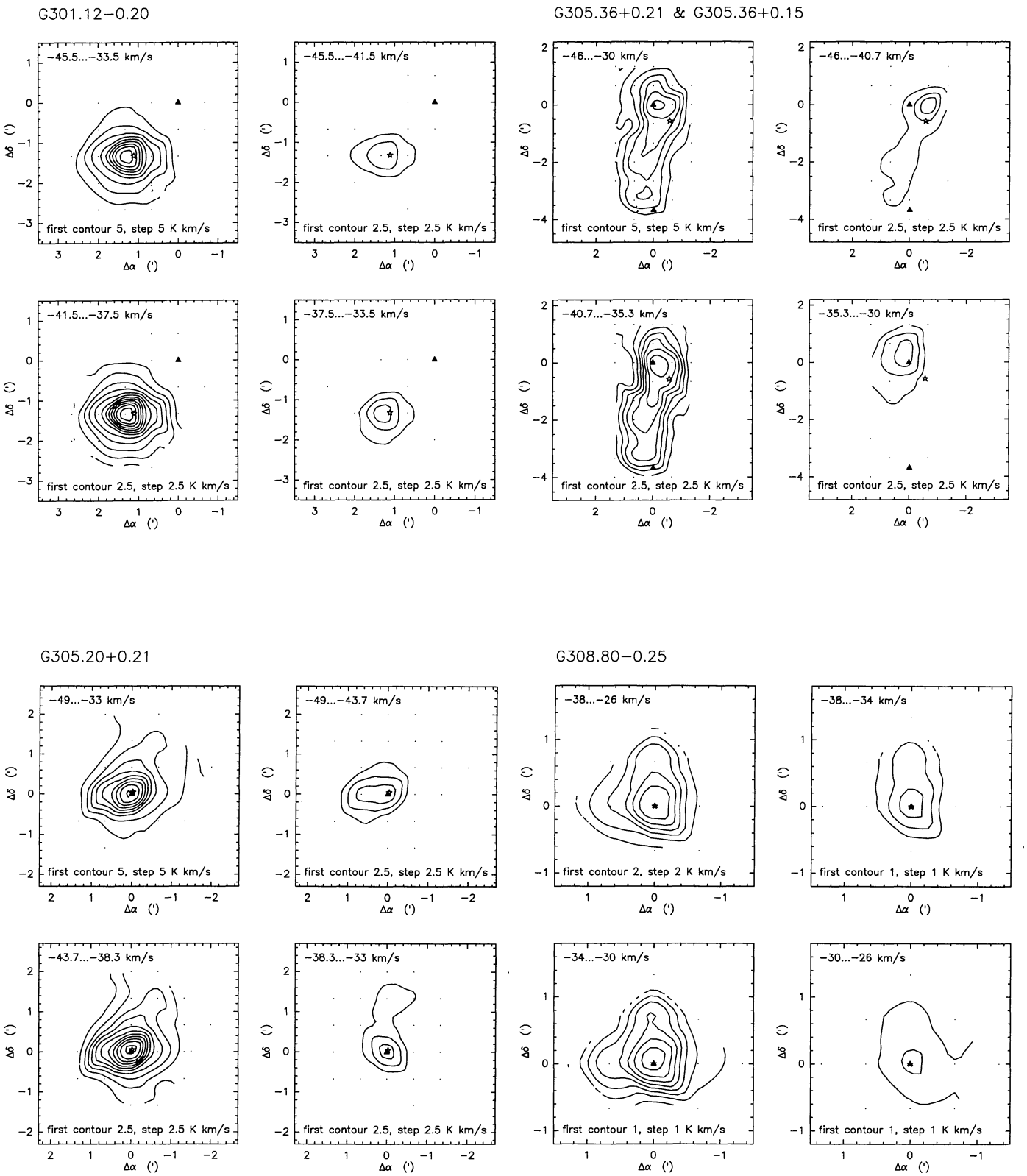

Fig. 1. continued

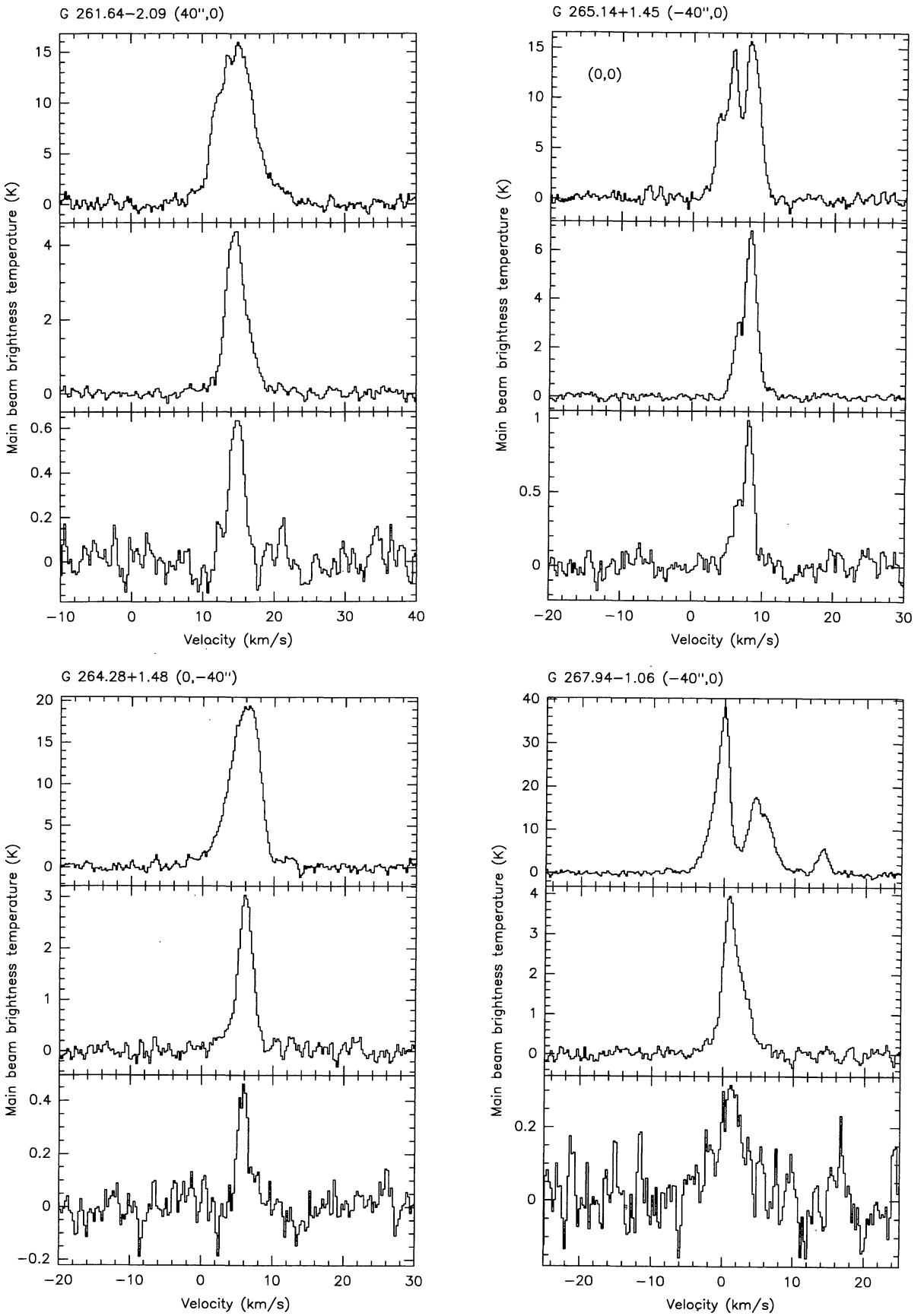

Fig. 2. The source spectra in the CO $J = 1-0$ (upper panels), CS $J = 2-1$ (middle panels) and $C^{34}S$ $J = 2-1$ (lower panels) lines at the indicated grid positions (closest to the CS emission peaks)

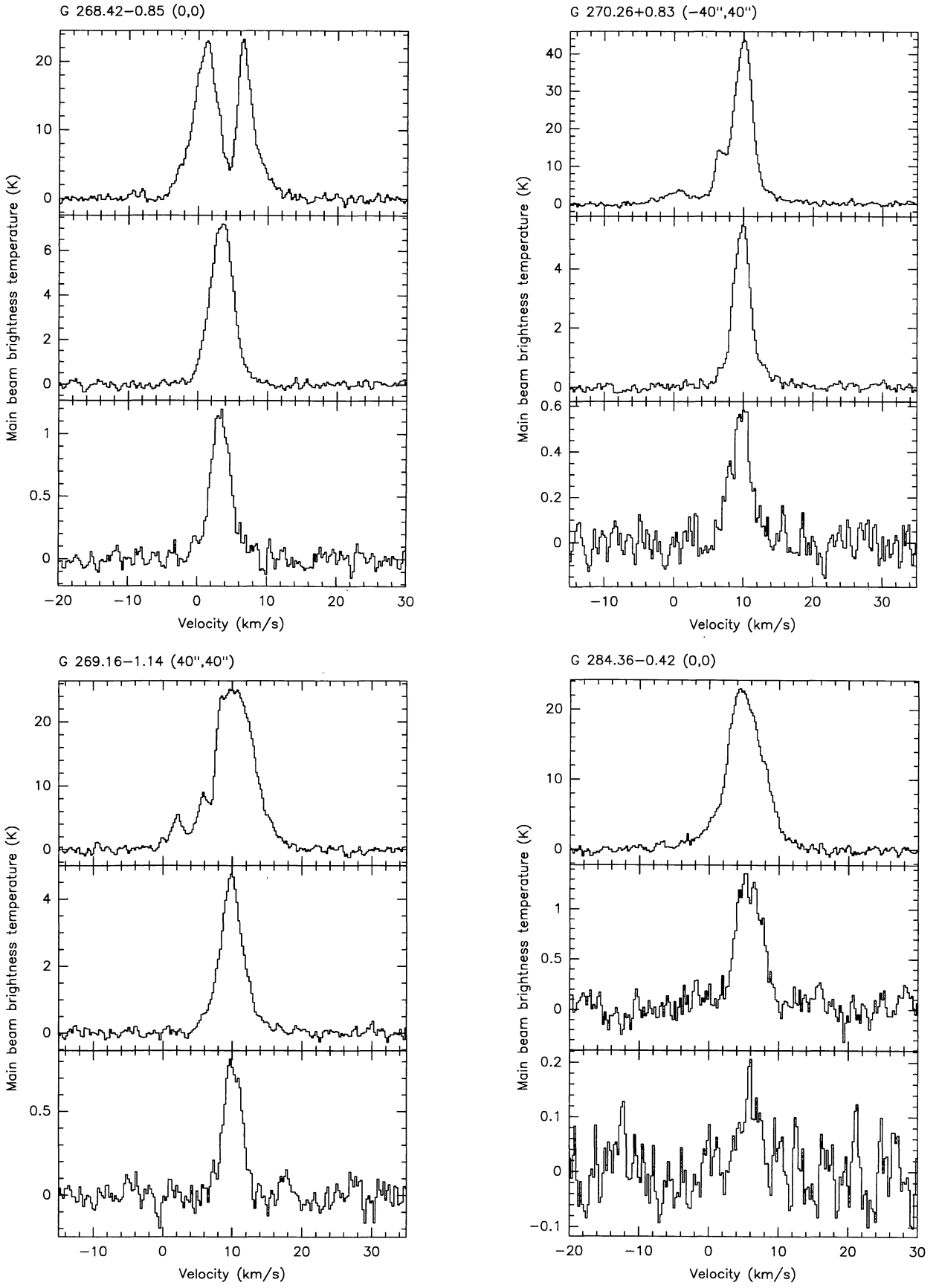

Fig. 2. continued

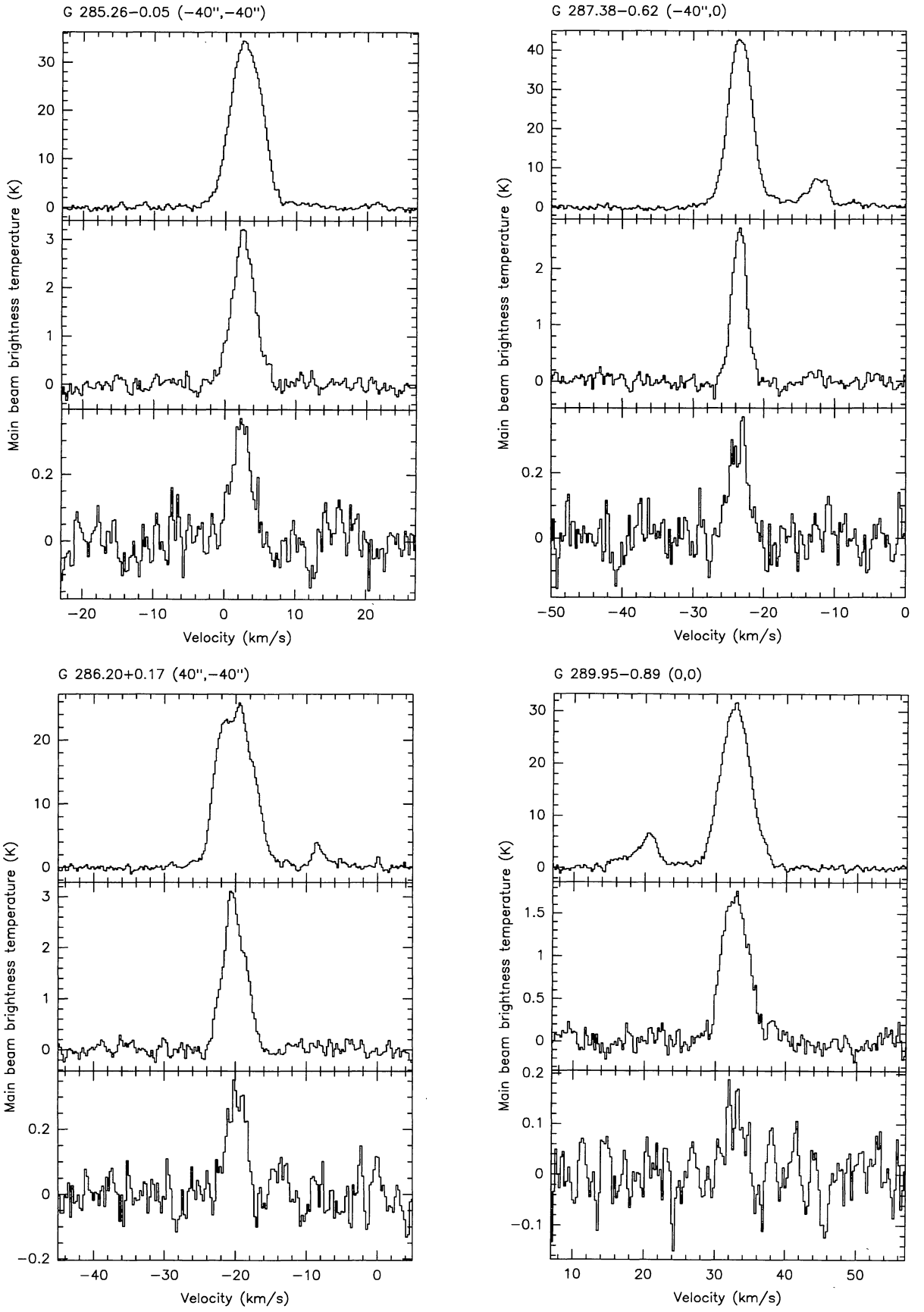

Fig. 2. continued

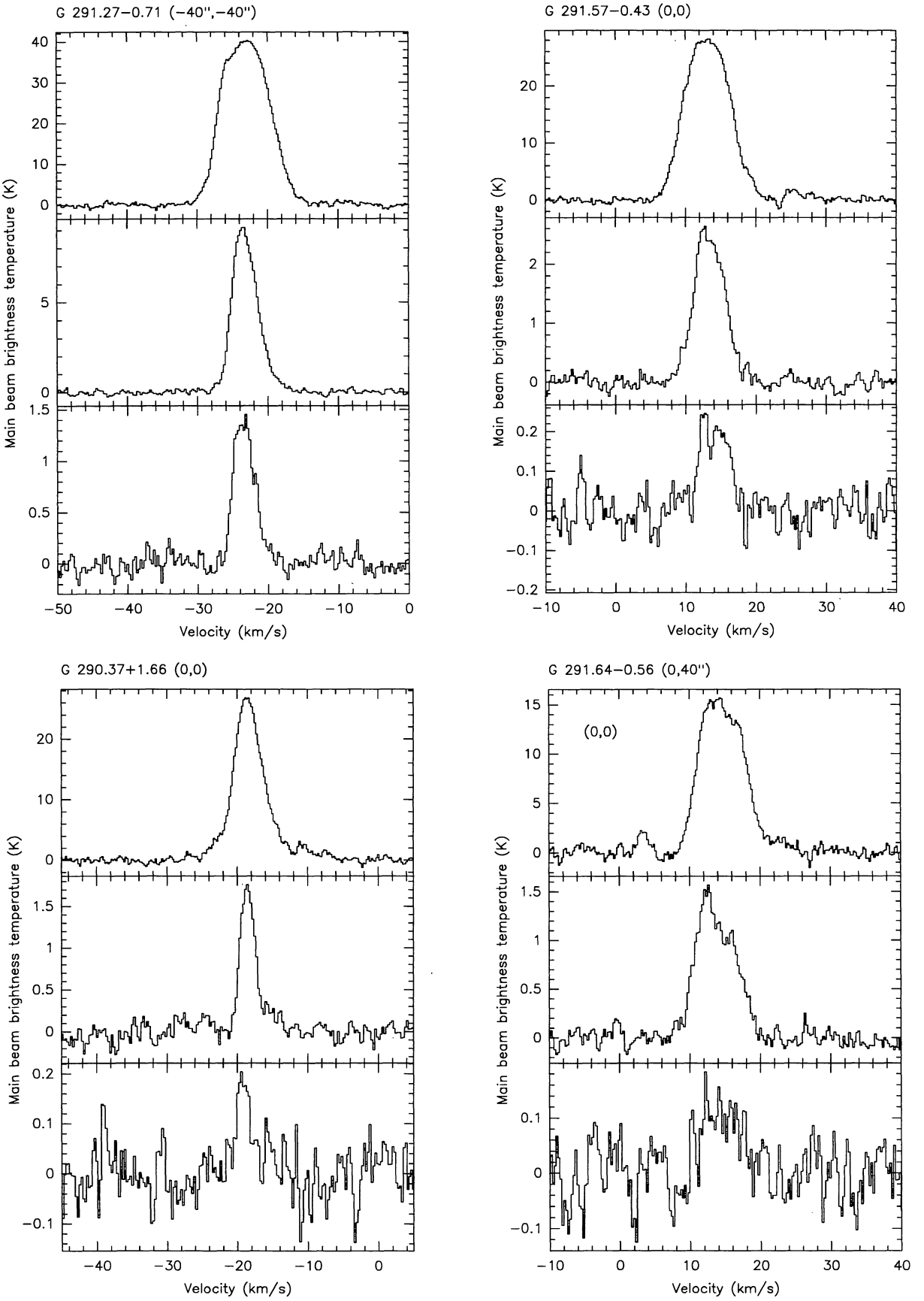

Fig. 2. continued

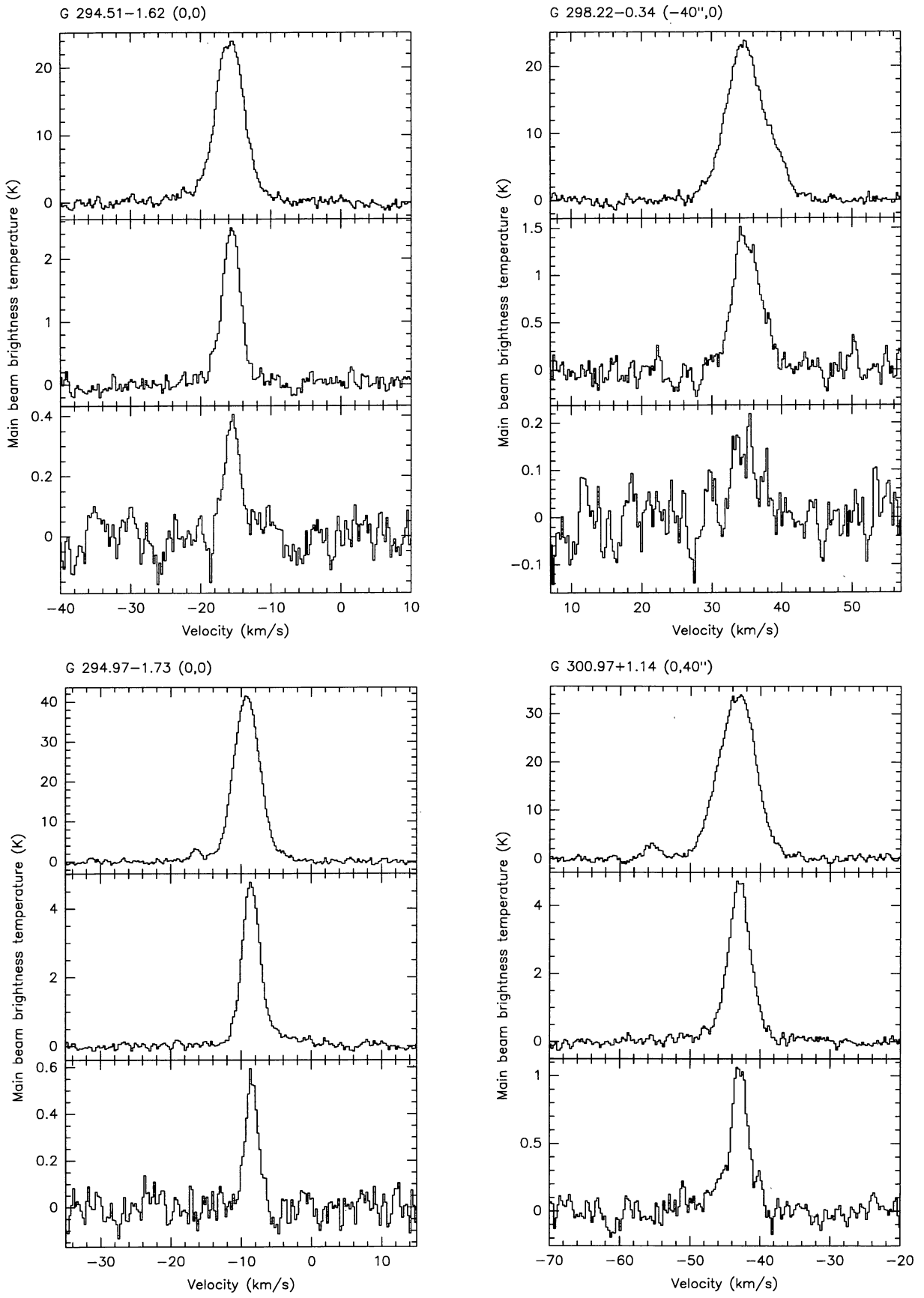

Fig. 2. continued

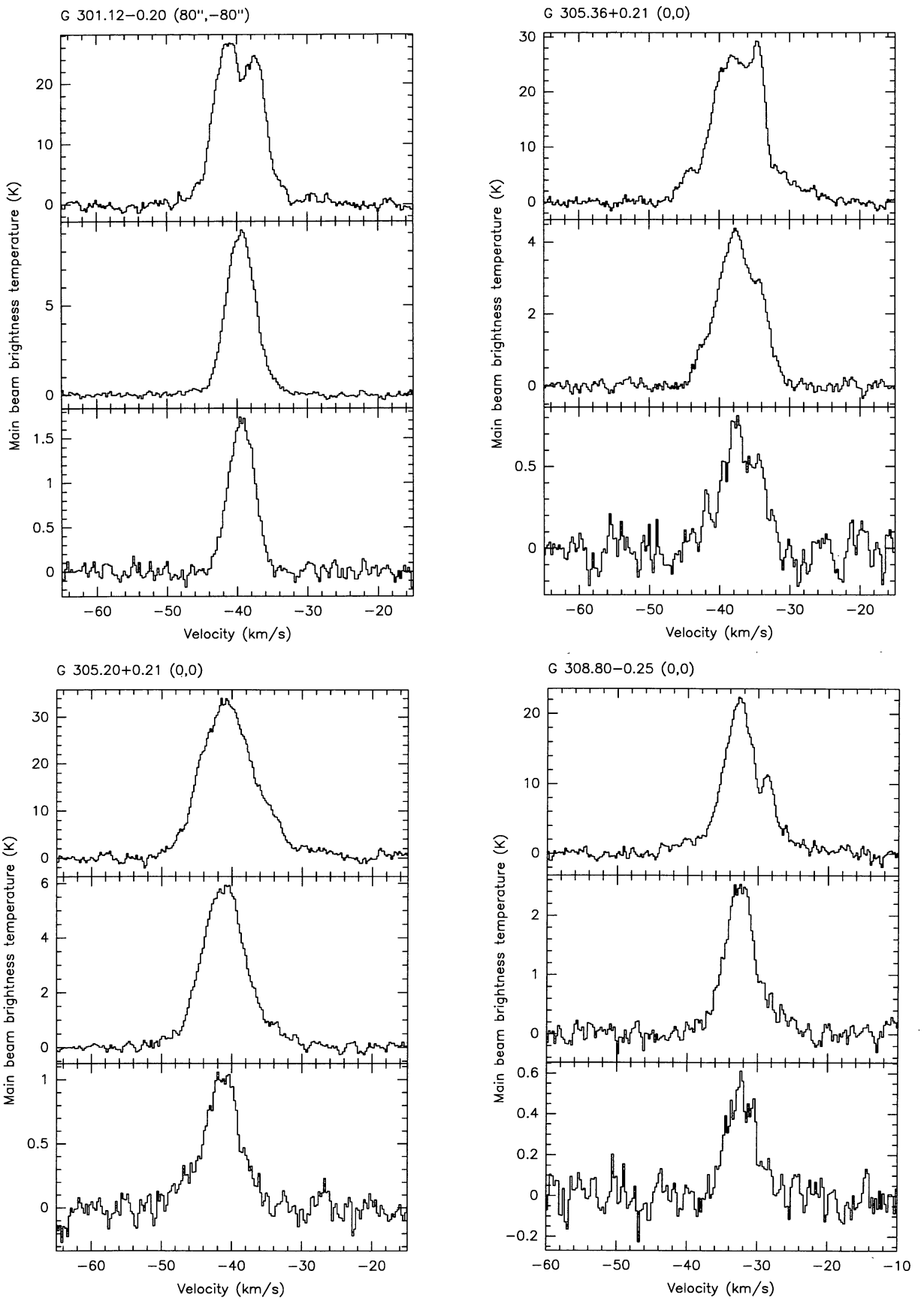

Fig. 2. continued

Table 2. CS and $C^{34}S$ line areas and gaussian line parameters at the indicated positions of the sources along with the peak CO main beam brightness temperatures. The numbers in the brackets are the statistical uncertainties in the last digits (standard deviations)

			CS				$C^{34}S$				CO
Source	$\Delta\alpha$ ($''$)	$\Delta\delta$ ($''$)	$\int T_{mb}dv$ (K·km/s)	T_{mb} (K)	V_{LSR} (km/s)	ΔV (km/s)	$\int T_{mb}dv$ (K·km/s)	T_{mb} (K)	V_{LSR} (km/s)	ΔV (km/s)	T_{mb} (K)
G 261.64−2.09	40	0	16.4(2)	2.44(31)	14.35(05)	2.27(09)	1.74(10)	0.65(03)	14.77(06)	2.4(2)	16
				2.16(17)	15.14(09)	4.30(17)					
G 264.28+1.48	0	−40	9.1(2)	2.71(17)	6.07(03)	2.18(08)	0.90(07)	0.44(03)	5.84(07)	1.8(2)	19
				0.33(05)	5.13(49)	7.5(20)					
G 265.14+1.45	−40	0	17.6(2)	8.7(3)	7.70(02)	2.55(03)	2.31(08)	2.4(11)	7.45(08)	2.0(2)	16[a]
				−4.7(5)	7.25(02)	1.28(06)		−1.9(14)	7.29(06)	1.5(2)	
G 267.94−1.06	−40	0	13.2(2)	6.3(9)	1.66(06)	3.00(11)	1.61(15)	0.26(03)	1.13(24)	5.4(7)	38
				−3.7(15)	2.04(05)	1.96(18)					
G 268.42−0.85	0	0	30.2(2)	7.25(04)	3.40(01)	3.88(03)	4.39(09)	1.15(02)	3.33(03)	3.4(1)	23
G 269.16−1.14	40	40	19.9(2)	2.49(23)	9.97(05)	5.31(28)	2.53(09)	0.80(03)	10.08(05)	3.0(1)	25
				2.19(52)	9.83(03)	2.38(22)					
G 270.26+0.83	−40	40	19.2(2)	4.80(02)	9.76(01)	2.56(02)	2.11(10)	0.55(02)	9.66(08)	3.5(2)	44
				0.74(03)	10.42(15)	7.61(38)					
G 284.36−0.42	0	0	7.3(2)	1.31(04)	5.69(07)	4.43(15)	0.48(08)	0.15(02)	5.97(28)	3.2(6)	23
G 285.26−0.05	−40	−40	12.1(2)	3.05(04)	2.57(02)	3.73(06)	1.18(09)	0.35(02)	2.36(10)	3.2(2)	34
G 286.20+0.17	40	−40	11.1(2)	2.58(05)	−20.10(04)	3.89(07)	1.01(08)	0.33(02)	−19.85(10)	2.9(2)	26
				0.72(15)	−20.70(06)	1.02(15)					
G 287.38−0.62	−40	0	6.7(2)	2.75(05)	−23.45(02)	2.43(05)	0.98(08)	0.30(02)	−23.54(11)	3.1(2)	43
G 289.95−0.89	0	0	8.2(2)	1.74(04)	32.76(04)	4.41(10)	0.36(07)	0.14(02)	32.78(21)	2.9(4)	32
G 291.27−0.71	−40	−40	40.8(2)	7.24(16)	−23.94(03)	3.15(04)	5.28(14)	1.44(04)	−23.47(04)	3.4(1)	40
				3.94(15)	−21.89(07)	3.84(13)					
G 290.37+1.66	0	0	5.1(2)	1.79(09)	−18.58(05)	2.31(11)	0.41(07)	0.19(02)	−19.16(14)	2.4(4)	27
				0.24(07)	−15.34(47)	3.1(11)					
G 291.57−0.43	0	0	13.8(2)	2.42(04)	13.48(05)	5.12(09)	1.03(10)	0.22(02)	13.93(15)	4.7(3)	28
				0.52(11)	12.13(09)	1.23(21)					
G 291.64−0.56	0	40	9.4(2)	1.42(11)	12.27(13)	3.84(21)	0.73(10)	0.12(01)	14.45(35)	6.0(7)	16[a]
				0.88(11)	16.16(20)	3.74(32)					
G 294.51−1.62	0	0	8.9(2)	2.26(16)	−15.61(03)	2.79(10)	1.01(08)	0.38(03)	−15.52(09)	2.7(2)	24
				0.26(05)	−16.34(47)	7.5(14)					
G 294.97−1.73	0	0	17.2(1)	4.42(08)	−8.62(01)	2.82(04)	1.22(07)	0.55(03)	−8.53(05)	2.2(1)	41
				0.40(03)	−6.17(35)	9.28(62)					
G 298.22−0.34	−40	0	7.1(2)	1.41(04)	35.02(06)	4.72(14)	0.68(09)	0.15(02)	34.81(24)	4.6(7)	24
G 300.97+1.14	0	40	20.6(2)	4.32(14)	−42.97(02)	3.52(07)	3.82(09)	0.88(14)	−42.86(05)	2.4(2)	34
				0.34(03)	−44.12(25)	12.0(16)		0.23(04)	−44.17(70)	7.8(14)	
G 301.12−0.20	80	−80	47.9(2)	9.08(04)	−39.44(01)	4.84(02)	7.83(12)	1.72(02)	−39.39(03)	4.3(1)	27
G 305.20+0.21	0	0	47.3(2)	4.90(24)	−41.32(03)	6.28(11)	6.37(18)	0.99(03)	−41.37(07)	6.2(2)	34
				1.11(12)	−39.75(27)	12.4(6)					
G 305.36+0.21	0	0	31.1(2)	4.11(05)	−37.68(04)	6.53(09)	4.26(20)	0.69(02)	−37.09(12)	6.5(3)	29
				1.10(12)	−33.67(05)	2.11(16)					
G 308.80−0.25	0	0	14.7(2)	1.87(21)	−32.71(06)	3.92(21)	2.60(15)	0.51(03)	−32.27(12)	4.9(3)	22
				0.72(10)	−31.70(33)	9.08(68)					

[a](0,0) position

cases. It means that the variations of the CS line area in objects of this kind are not very large ($\lesssim$ a factor of 10). The variations of the CS column density should be of the same order of magnitude.

It is worth noting that the maser velocities (Table 1) differ significantly from the CS velocities (Table 2) in many cases. The histogram of $V(H_2O) - V(CS)$ is plotted in Fig. 4.

For G 268.42−0.85 the difference reaches 62 km/s and for G 291.28−0.71 100 km/s. The standard deviation of the velocity difference is 23 km/s (7 km/s without these two extreme cases). It is interesting to note that there is an asymmetry in the velocity difference distribution with more negative radial velocities relative the CS cores. The mean difference $V(H_2O) - V(CS)$ is -8.4 ± 4.3 km/s (-2.6 ± 1.4 km/s without G 268.42−0.85 and G 291.28−0.71). If this asymmetry is real it could mean that the maser emission is beamed preferably in the direction of its movement relative the parent cloud.

The examination of the IRAS point source and small scale structure catalogues (IRAS catalogs 1988) demonstrates that most of these masers and CS sources are probably associated with strong IRAS point sources; 2 masers are associated with a small scale structure source. The list of these sources located within the studied regions is presented in Table 3. The positions of the point sources are indicated in Fig. 1.

No appropriate IRAS association could be found for 2 masers. However, the CS emission was detected in both cases. Most frequently the nominal IRAS positions are very close to the maser positions (in fact for some masers these IRAS positions have been adopted, apparently). In

Table 3. IRAS point sources and small scale structure sources probably associated with the masers and CS sources. The flux quality flags are shown following the notation in the IRAS point source and small scale structure catalogues

Source	IRAS PSC, SSSC										
	Name	α	δ	$F_{12\mu}$		$F_{25\mu}$		$F_{60\mu}$		$F_{100\mu}$	
	(^{h})(^{m}) (°)(′)	(^{s})	(″)	(Jy)		(Jy)		(Jy)		(Jy)	
G 261.64−2.09	08303−4303	23.2	31	3.52		30.36		418.52		1012.41	
G 264.28+1.48	08546−4254	39.0	11	29.31		193.60		1343.72		2098.23	:
G 265.14+1.45	08576−4334	36.9	02	66.78	:	582.01	:	8333.44	:	15746.73	
G 267.94−1.06	08573−4718	22.5	54	973.15		4279.71	S	3.92	L	31568.23	S
G 268.42−0.85	09002−4732	12.1	07	120.52		1962.02		11876.81		14706.72	
G 269.11−1.12	09017−4814	44.3	32	22.38		134.38		1804.05	:	7755.96	L
	09017−4813	44.2	50	13.28		90.67	:	892.56	L	6022.47	L
G 269.16−1.14	09018−4816	51.6	43	8.26	:	138.81		1835.00	:	7755.96	L
	09017−4819	46.3	24	8.12		13.89		131.08	L	7755.96	L
G 270.26+0.83	09149−4743	57.9	50	18.74		118.37		928.24		1909.90	
G 284.17−0.79	10197−5750	44.8	32	200.00		1091.64		558.30		272.60	L
G 284.30−0.34	X1022−575	19.7	31′21	4050	B	20600	F	41500	F	58200	F
G 284.36−0.42	X1022−575	19.7	31′21	4050	B	20600	F	41500	F	58200	F
G 285.26−0.05	10295−5746	35.4	40	92.97		1061.51		9280.39		13436.87	
G 286.20+0.17	10365−5803	34.8	22	7.24	L	85.64		1173.00		2782.41	
G 287.38−0.62	10414−5919	24.7	47	21.09		2.61	L	4653.14	L	17096.17	S
G 289.95−0.89	10591−6040	07.4	54	15.89		93.34		707.58		1263.06	
G 291.27−0.71	11097−6102	44.7	17	391.01		5956.91	:	10903.76	S	38551.69	S
	11094−6105	24.8	30	17.09		129.41		614.84	L	61.83	L
G 291.28−0.71	11097−6102	44.7	17	391.01		5956.91	:	10903.76	S	38551.69	S
	11094−6105	24.8	30	17.09		129.41		614.84	L	61.83	L
G 290.37+1.66	11101−5829	07.4	60	9.00		130.35		618.19		750.21	
G 291.57−0.43											
G 291.64−0.56											
G 294.51−1.62	11332−6258	12.9	15	6.93		37.40		479.08		1162.64	L
G 294.97−1.73	11368−6312	51.6	09	13.14		167.11		1282.88		3401.93	
G 298.22−0.34	12073−6233	21.7	15	577.39	:	4084.29		10672.38		11344.59	
G 299.02+0.15	12146−6212	41.8	14	3.78		26.12		299.76		636.71	:
G 300.97+1.14	12320−6122	01.7	52	79.47	:	350.61		5242.05		7977.47	
G 301.12−0.20	12326−6245	41.0	57	7.79	:	308.89		7556.82		9296.37	
G 305.20+0.21	13079−6218	59.6	47	28.32	:	249.72		3166.58	:	8163.55	:
G 305.36+0.15	13092−6218	16.3	36	125.18		834.62		8860.59	L	19253.68	
G 305.36+0.21	13092−6218	16.3	36	125.18		834.62		8860.59	L	19253.68	
G 308.80−0.25	13134−6242	27.2	56	6.97		79.07		1485.94		2624.69	

general the CS peaks seem to be located closer to the IR sources (e.g., G 301.12−0.20) or between the IR and maser positions (e.g., G 287.38−0.62) but the uncertainties of these positions do not enable to make a firm conclusion.

4.2. *Spatial and kinematic structure*

The morphological (spatial and kinematic) appearances of the sources vary significantly. We can divide them roughly into three groups: (A) sources with apparently simple nearly spherical structure without noticeable velocity gradients, (B) elongated sources with perhaps a smooth velocity gradient and (C) apparently multicomponent sources with a complicated spatial structure. There are also intermediate cases. Of course the appearance of the source can depend on the distance to it and on the viewing angle. We should not see much structure in the very remote sources. However, from the available distance estimates we do not see any dependence of this kind. Approximately 40−50% of the sources can be classified as belonging to the group A, 20−40% to the group B and 20−25% to the group C.

As mentioned above the peaks of the CS emission are usually located closer to the IR sources than to the masers. Anyway, in many cases they are shifted by up to $\sim 1'$ from the IR positions, too.

Only a few cores demonstrate velocity gradients which can be considered indicative of rotation (these cores have an elongated structure). Most of the CS lines at the peak

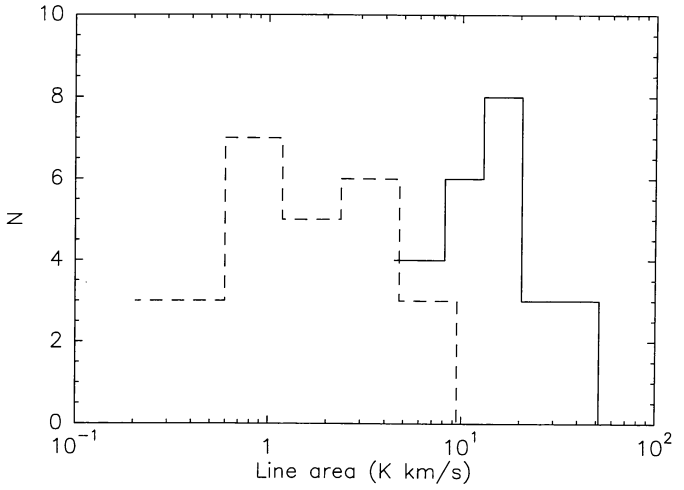

Fig. 3. Histograms of the CS (solid line) and $C^{34}S$ (dashed line) line area distributions at the peak positions of the sources

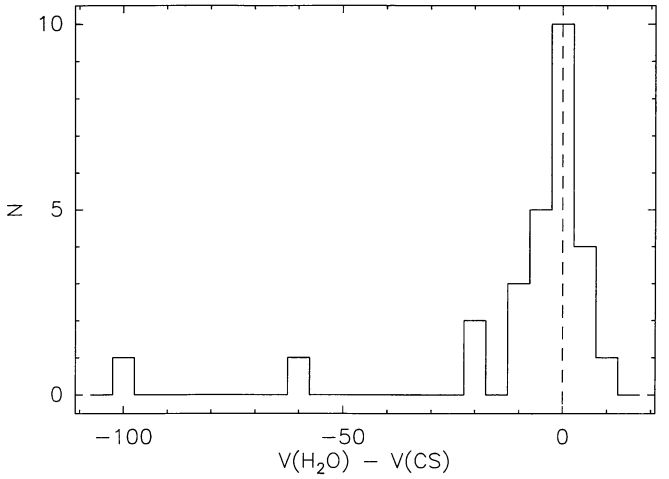

Fig. 4. Histogram of the differences between the H_2O and CS velocities

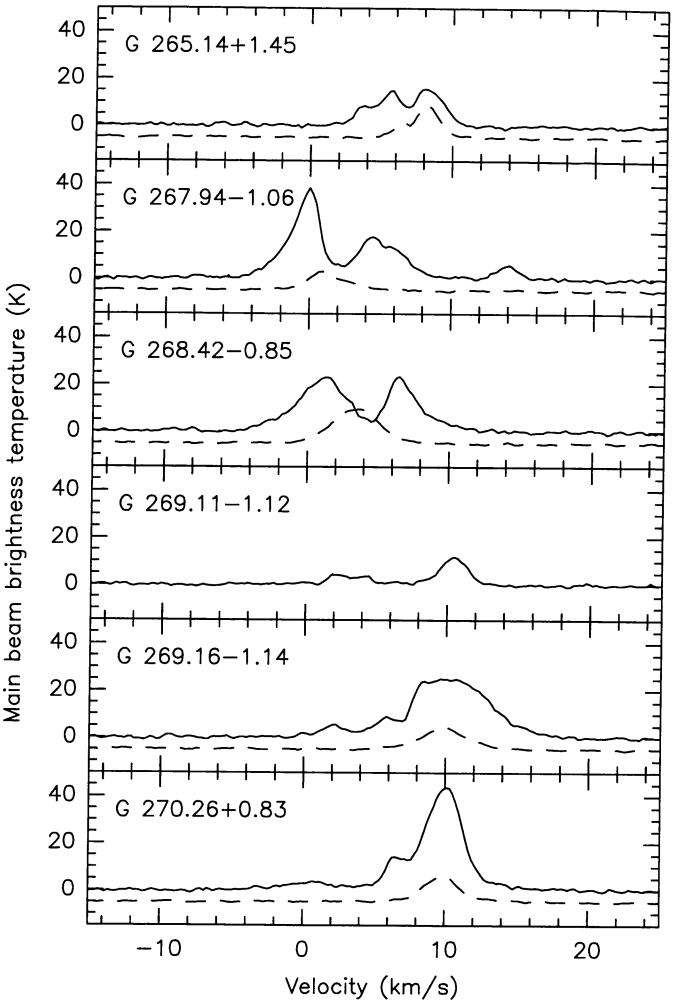

Fig. 5. CO spectra with prominent self-absorption in several sources plotted on the same velocity scale (solid lines). The dashed lines represent the CS spectra (scaled by a factor of 2)

positions (see Fig. 2) have broad wings extending up to ~ 10 km/s from the line centroids at the detectable level (~ 0.2 K). They indicate probably dense high velocity flows in these objects. We cannot investigate the spatial structure of this wing emission with our present observing material due to a higher noise level in the spectra obtained at other positions. Similar but broader wings can be seen also in the corresponding CO spectra.

4.3. *Absorption features*

Several CO and CS lines are clearly affected by a foreground absorption. In one case (G 265.14+1.45) the absorption is rather obvious even in the $C^{34}S$ line. The absorption is sometimes very deep. In G 268.42−0.85 the CO brightness temperature in the dip is only ~ 4 K. It means that it is caused by a very low excited molecular gas on the line of sight which contains a sufficient amount of CS molecules too. There is the question whether this absorbing material is intimately related with the core or it is just an accidental foreground cloud. We believe that the latter explanation is preferable. There are the following arguments in favour of this point of view:

Only a rather small part of the sources from our sample demonstrates such absorption features. Moreover, almost all of them are concentrated within a few degrees around the longitude $l \approx 270°$. In Fig. 5 we plot the CO and CS spectra of these clouds on the same velocity axis including also the CO spectrum for G 269.11−1.12 where no CS emission was detected. It is easy to see that the absorption in different sources occurs sometimes at similar velocities which correspond also to weak CO emission features in some of these spectra. So, it is reasonable to assume that there is an extended low excitation foreground cloud (or clouds) in this direction. It may be of relevance that we are looking here almost along the tangential direction where

the radial velocities of the clouds are close to zero. An occasional velocity overlap with a foreground cloud can most easily happen in this direction (except for the directions to the galactic centre and anti-centre of course).

4.4. $C^{34}S$ column densities

The LTE estimates of the $C^{34}S$ column densities calculated from the $C^{34}S$ line areas (Sect. 2.3) are presented in Col. (2) of Table 4. As was shown in Paper I the LTE estimates are usually rather close to the LVG estimates which require a knowledge of the cloud temperature and density.

4.5. *Sizes, masses and densities*

For sources with available distances (either spectrophotometric or kinematic) we estimated linear sizes, masses and densities in the same way as in Paper I (the expression for the mass evaluation as printed in Paper I should be corrected by a factor of d^2 in the notation of the present paper). The results are presented in Table 4. For sources with both spectrophotometric and kinematic distances determined the most recent spectrophotometric values were used. In fact, in the cases where the comparison is possible these distances are reasonably close to each other. For G 294.51−1.62 and G 308.80−0.25 the near kinematic distances were used. The examination of these results reveals in particular the size-density and size-linewidth correlations similar to those found in Paper I. However, we leave the detailed analysis of these data for the forthcoming publications.

Table 4. $C^{34}S$ column densities, sizes, mean densities and masses of the cores derived from the CS maps and $C^{34}S$ line areas. The numbers in the brackets are the statistical uncertainties in the last digits (standard deviations)

Source	log $N_L(C^{34}S)$ (cm^{-2})	L (pc)	log $\bar{n}$ (cm^{-3})	M ($M_\odot$)
G 261.64−2.09	12.92(02)	1.1	4.15	894
G 264.28+1.48	12.64(03)	1.8	3.65	1320
G 265.14+1.45	13.04(01)	1.2	4.24	1410
G 267.94−1.06	12.89(04)	1.4	4.00	1500
G 268.42−0.85	13.32(01)	0.6	4.84	607
G 269.16−1.14	13.08(02)	1.5	4.17	2460
G 270.26+0.83	13.00(02)	1.8	4.01	3040
G 284.36−0.42	12.36(07)	1.5	3.46	456
G 285.26−0.05	12.75(03)	3.3	3.49	5780
G 286.20+0.17	12.69(03)			
G 287.38−0.62	12.67(04)	1.7	3.70	1290
G 289.95−0.89	12.24(08)	2.1	3.19	693
G 291.27−0.71	13.40(01)	2.6	4.25	15800
G 290.37+1.66	12.30(07)	1.2	3.49	258
G 291.57−0.43	12.69(02)	5.6	3.20	14500
G 291.64−0.56	12.54(06)	3.9	3.21	5030
G 294.51−1.62	12.69(03)	1.0	3.97	425
G 294.97−1.73	12.77(02)	1.6	3.83	1410
G 298.22−0.34	12.52(05)	4.8	3.10	7170
G 300.97+1.14	13.26(01)	1.2	4.45	2420
G 301.12−0.20	13.57(01)			
G 305.20+0.21	13.49(01)	1.8	4.49	9860
G 305.36+0.21	13.31(02)	3.0	4.09	17800
G 308.80−0.25	13.10(02)	1.2	4.27	1770

5. Summary and conclusions

We have presented the results of the CS $J = 2 - 1$ survey towards 30 non-stellar molecular masers in the longitude range $l = 260° - 310°$ (29 H_2O and H_2O/OH masers and one OH maser). We detected and mapped 24 CS emitting regions probably associated with 27 H_2O masers. The $C^{34}S$ $J = 2 - 1$ and CO $J = 1 - 0$ lines were also observed at the grid positions closest to the CS peaks. We estimated the $C^{34}S$ column densities in the LTE approximation and calculated kinematic distances to the sources. Most of the cores are associated with strong IRAS point sources, two cores are associated with an IRAS small scale structure source.

The morphological structure of the sources varies significantly from single highly concentrated cores to complicated multicomponent emission regions. There is no clear dependence of this morphology on the distance. The CS spectra at the peak positions obtained with higher signal-to-noise ratios demonstrate extended wings in many cases.

The differences between the maser and CS velocities reach several tens of km/s and, on the average, the maser emission is blue-shifted relative to the CS emission.

There are deep absorption features in the CO and CS profiles of several sources concentrated mainly towards $l \approx 270°$. We argue that this can be due to an extended low-excitation foreground cloud.

For the cores with available distances (either spectrophotometric or kinematic) the sizes, masses and mean densities have been estimated.

Acknowledgements. We thank L. Haikala for the help with the IRAS identifications, J. Harju for the help with the data reduction and A. Lapinov for collecting relevant published data on several sources. I.Z. is very grateful to ESO for support by the ESO C&EE grant A–02–001 and to the Helsinki University Observatory for the hospitality during the data reduction and the paper preparation stages. He was also supported in part by grant R95000 from the International Science Foundation and grant 94–02–04861–a from the Russian Foundation for Basic Research.

References

Avedisova V.S., Palouš J. 1989, Bull. Astron. Inst. Czechosl. 40, 42

Booth R.S., Delgado G., Hagström M. et al. 1989, A&A 216, 315
Brand J., Blitz L. 1993, A&A 275, 67
Braz M.A., Epchtein N. 1983, A&AS 54, 167
Braz M.A., Scalise Jr. E., Gregorio Hetem J.C., Monteiro do Vale J.L., Gaylard M. 1989, A&AS 77, 465
Fich M., Blitz L., Stark A.A. 1989, ApJ 342, 272
Georgelin Y.M., Georgelin Y.P. 1976, A&A 49, 57
IRAS Catalogs 1988, Infrared Astronomical Satellite (IRAS) Catalogs and Atlases, NASA, RP-1190
Plume R., Jaffe D.T., Evans II N.J. 1992, ApJS 78, 505
Plume R., Jaffe D., Evans II N.J., Martín-Pintado J., Gómez-González J. 1993, A multi-transition study of CS in regions of massive star formation, eds. J.P. Cassinelli, E.B. Churchwell, Massive Stars: Their Lives in the Interstellar Medium, ASP Conf. Ser. 35, 93
Scalise Jr. E., Rodríguez L.F., Mendoza-Torres E. 1989, A&A 221, 105
The SEST Handbook 1993. Operating Manual No. 19, European Southern Observatory
Walmsley C.M., Güsten R. 1994, Conditions in regions of high mass star formation, ed. T.L. Wilson, The Structure and Context of Molecular Clouds, in press
Winnewisser G., Cook R.L. 1968, J. Mol. Spectrosc. 28, 266
Zinchenko I., Forsström V., Lapinov A., Mattila K. 1994, A&A 288, 601 (Paper I)